Dietary restriction promotes neuronal resilience via ADIOL

Ana Guijarro-Hernández[1], Shinja Yoo[1], George A. Lemieux[1], Sena Komatsu[1], Wei I. Jiang[2], Abdullah Q. Latiff[1], Rishika R. Patil[1], Dengke K. Ma[1,2], and Kaveh Ashrafi[1]

1. Department of Physiology, University of California, San Francisco, San Francisco, CA 94143, USA
2. Cardiovascular Research Institute, University of California San Francisco, San Francisco, CA 94158, USA

Correspondence: kaveh.ashrafi@ucsf.edu (K.A.)

GRAPHICAL ABSTRACT

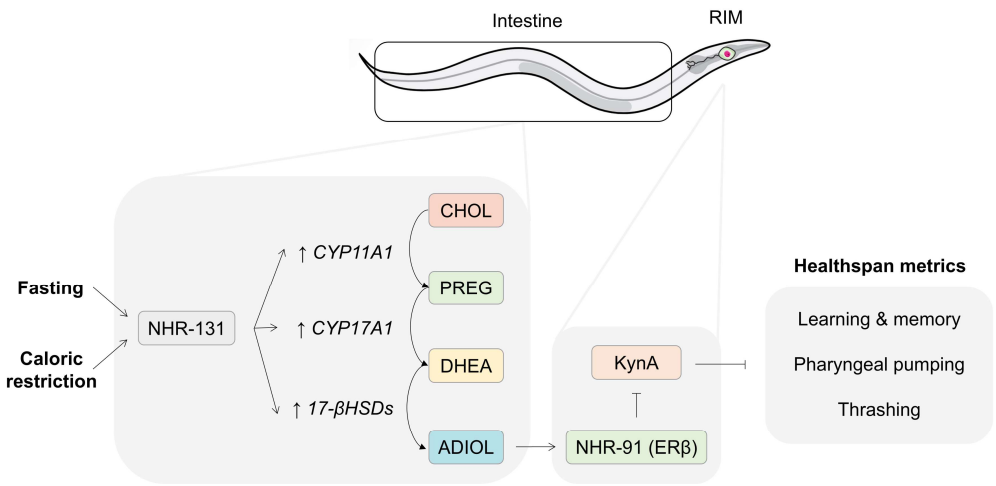

ABSTRACT

The steroid hormone 5-androstene-3β,17β-diol (ADIOL) was discovered in humans nearly a century ago, yet its physiological roles remain poorly defined. Here, we show that fasting and caloric restriction, two forms of dietary restriction, induce transcriptional upregulation of genes encoding CYP11A1, CYP17A1, and 17β-hydroxysteroid dehydrogenase family enzymes, promoting ADIOL biosynthesis. ADIOL, in turn, acts on the nervous system to reduce levels of kynurenic acid, a neuroactive metabolite linked to cognitive decline and neurodegeneration. This effect requires NHR-91, the *C. elegans* homolog of estrogen receptor β, specifically in the RIM neuron, a key site of kynurenic acid production. Consistent with the known benefits of fasting and caloric restriction on healthspan, enhancing ADIOL signaling improves multiple healthspan indicators during aging. Conversely, animals deficient in ADIOL signaling exhibit reduced healthspan under normal conditions and in genetic models of caloric restriction, underscoring the functional significance of this pathway. Furthermore, ADIOL suppresses cellular stresses induced by the Alzheimer's-associated APOE4 variant, highlighting its potential as a neuroprotective agent. Notably, ADIOL does not significantly impact lifespan, indicating that its healthspan benefits are not simply a byproduct of lifespan extension. Together, these findings establish a physiological role for ADIOL in mediating the neuroprotective and pro-healthspan effects of fasting and caloric restriction and suggest that boosting ADIOL signaling may help narrow the gap between lifespan and healthspan. This positions ADIOL as a promising mimetic of dietary restriction effects on healthspan that could be used as a therapeutic strategy for age-related neurodegenerative conditions.

INTRODUCTION

A central goal in aging research is to close the lifespan–healthspan gap, which refers to the difference between how long an organism lives (lifespan) and the duration over which it maintains robust physiological functions, collectively referred to as healthspan (1).

Steroid hormones are lipophilic molecules derived from cholesterol that regulate a wide range of physiological processes. Classic examples include cortisol, a glucocorticoid that modulates stress responses, metabolism, and immune function; and the sex steroids testosterone (an androgen) and 17β-estradiol (E2) (an estrogen), which govern sexual development and many other biological functions (2).

Among steroid hormones, 5-androstene-3β,17β-diol (ADIOL) was discovered in humans nearly a century ago but has received limited attention. Often regarded as a minor byproduct of testosterone and E2 biosynthesis, ADIOL is produced from dehydroepiandrosterone (DHEA), a common precursor for all three steroids (3; **Supplementary Fig. 1a**). In mammals, DHEA is synthesized in both gonads and adrenal glands, and enzymatic conversions involving CYP11A1, CYP17A1, and 17β-HSDs direct it toward specific downstream products (3).

Initially classified as an androgen, ADIOL was found to possess only ~0.21% of the androgenic activity of testosterone in rats (4). A 1997 study showed that ADIOL binds to both estrogen receptor β (ERβ) and estrogen receptor α (ERα), with ~3-fold higher affinity for ERβ (5), establishing it as an estrogenic compound. Unlike E2, which shows strong sex dimorphism in circulating levels, ADIOL is present at relatively similar low-nanomolar levels in both sexes (6,7). Though its binding affinity is weaker than that of E2 (~6% for ERα and ~17% for ERβ) (5), its relatively high abundance supports its function as an endogenous ERβ ligand. Furthermore, astrocytes and microglia can locally convert circulating DHEA into ADIOL (8), suggesting a mechanism for tissue-specific regulation of ADIOL versus E2 signaling.

Crucially, ADIOL and E2 differ in their downstream effects upon binding ERβ. ADIOL, but not E2, suppresses microglial inflammation by recruiting CtBP corepressor complexes to AP-1-dependent promoters via ERβ (8), demonstrating functionally distinct transcriptional outcomes.

We recently discovered that *C. elegans* also synthesizes ADIOL (9). As in mammals, ADIOL biosynthesis in *C. elegans* depends on cytochrome P450 enzymes and 17β-HSDs (9). These enzymes are transcriptionally regulated by NHR-131, which is prominently expressed in the intestine, a metabolically active tissue in *C. elegans* (9). Elevated ADIOL levels enhance pharyngeal pumping rate, the mechanism of food intake, and improve associative learning (9). The learning paradigm employed requires *C. elegans* orthologs of NMDA and AMPA glutamate receptors, as well as CaMKII kinase, and CREB, a transcription factor, underscoring the evolutionary conservation of pathways implicated in learning and memory (10-15).

Supporting the hypothesis that ADIOL acts via ERβ-like signaling, its effects on pumping rate and learning require NHR-91, the *C. elegans* homolog of ERβ. Notably, these effects are not mimicked by E2 or testosterone (9). In *nhr-91* mutants, ADIOL has no effects on pumping or learning behaviors, but restoring wild-type *nhr-91* expression specifically in RIM neurons fully rescues ADIOL responsiveness (9). RIM neurons have previously been identified as a key site for the production of kynurenic acid (KynA), a tryptophan-derived metabolite that inhibits NMDAR-dependent activity of distinct neurons implicated in regulations of pharyngeal pumping (AVA neurons) and learning (RIM neurons) **(Supplementary Fig. 1b–c)**. We find that ADIOL reduces KynA levels in *C. elegans*, thereby enhancing NMDAR-dependent neural functions (9). KynA similarly affects mammalian cognition: lower KynA levels are associated with improved cognition, whereas elevated KynA impairs learning and memory (16-23).

Once considered mere metabolic byproducts, kynurenine pathway (KP) metabolites such as KynA are now recognized as active signaling molecules involved in numerous pathological processes (24-29). Altered KP signaling has been implicated in neurodegenerative disorders, and modulating KP metabolites is an emerging therapeutic strategy (24,30). Additionally, KP has been linked to healthspan regulation in mammals (31). For instance, elevated kynurenine (Kyn), the precursor to KynA, is associated with sarcopenia (32), hip fractures (33,34), and cardiovascular disease (35) in older adults, and with muscle atrophy (36) and bone loss (37) in animal models.

In *C. elegans*, pharyngeal pumping and learning capacity are established behavioral readouts of healthspan (15,38). While our earlier ADIOL studies focused on day 1 adults, we have now systematically examined the effects of ADIOL during aging.

Moreover, we find that ADIOL biosynthesis is induced under fasting and caloric restriction (CR)-mimicking conditions, collectively referred to as dietary restriction (DR), and that increasing ADIOL levels broadly promotes healthspan. However, unlike CR, which extends lifespan, modulating ADIOL levels causes minimal changes in lifespan. These data suggest that ADIOL mediates the neural healthspan-promoting effects of DR, independent of lifespan extension.

In summary, our findings establish ADIOL as an endogenous steroid that regulates the kynurenine pathway and neural function via ERβ/NHR-91 signaling. By enhancing indicators of healthspan without extending lifespan, ADIOL emerges as a candidate for closing the lifespan–healthspan gap.

RESULTS

ADIOL links nutrient status to pharyngeal pumping and learning capacity via KynA reduction

The discovery of ADIOL in *C. elegans* was facilitated by a synthetic compound, F17, initially identified through an unrelated phenotypic screen (9,39). Epistasis analyses linked F17's activity to the kynurenine pathway metabolite kynurenic acid (KynA), and subsequent work revealed that NHR-131 and ADIOL mediate F17's effects **(Supplementary Fig. 1b)**. Given the synthetic nature of F17 and the limited understanding of NHR-131 function, we sought to identify physiological conditions that regulate ADIOL levels.

We hypothesized that nutritional status modulates ADIOL, based on prior observations that KynA levels are nutritionally sensitive (10,40). Specifically, neural KynA levels provide a mechanism through which *C. elegans* senses nutrient availability and adjusts pharyngeal pumping accordingly (40): *C. elegans* rapidly reduce pumping upon food removal and increase it when reintroduced to food. Notably, if *C. elegans* undergo a brief 2-hour fast before refeeding, they exhibit a transient hyperactivation of pumping. This behavioral pattern is regulated by KynA levels. Fasting-induced KynA reduction leads to NMDAR-dependent activation of AVA neurons, triggering a neuropeptide Y-like signaling axis (FLP-18–NPR-5), which promotes pharyngeal pumping via serotonergic pathways (40). KynA-deficient animals show elevated

pumping even when well-fed, while animals that cannot sufficiently reduce KynA levels fail to exhibit the post-fast pumping spike (40).

To determine if ADIOL contributes to fasting-induced KynA reduction, we examined pharyngeal pumping after fasting in animals lacking either NHR-91 (the ADIOL receptor) or NHR-131 (required for ADIOL biosynthesis). Unlike wild-type (WT) animals, *nhr-91* mutants failed to exhibit the hyperactivated pumping response after fasting, and *nhr-131* mutants showed only a minimal increase (**Fig. 1a**). Given that *nhr-131* regulates multiple steroidogenic enzymes, including *CYP17A1/cyp13A4*, these mutants likely have defects in the production of other steroids as well. To confirm that the phenotype was due to ADIOL deficiency, we administered exogenous ADIOL to *nhr-131* and *nhr-91* mutant animals. This fully restored the post-fasting pumping response to wild-type levels in *nhr-131* but not in *nhr-91* mutants **(Fig. 1b)**, consistent with the roles of NHR-131 and NHR-91 in ADIOL biosynthesis and response, respectively.

NHR-91, the *C. elegans* ortholog of ERβ, is expressed in multiple neuronal types, including the RIM and RIC neurons (9), as well as some non-neural cells (41). Both RIM and RIC neurons have been shown to regulate pharyngeal pumping (42) but only RIM neurons can generate KynA (10,40). To determine the site of ADIOL action in regulation of pharyngeal pumping, we used neuron-specific promoters to express *nhr-91* exclusively in RIM or RIC neurons in *nhr-91* mutants. ADIOL increased pumping when *nhr-91* was expressed in RIM neurons, but not when expressed in RIC neurons **(Fig. 1c),** pinpointing RIM neurons as the site of ADIOL action. Taken together, these findings support a model where fasting activates NHR-131, promoting ADIOL biosynthesis, which then binds to NHR-91 in RIM neurons to reduce KynA levels, thereby enhancing pharyngeal pumping **(Fig. 1d).**

To assess whether ADIOL's effects are sexually dimorphic, we measured pharyngeal pumping in hermaphrodites and males treated with ADIOL or F17, which elevates ADIOL levels (9). Both compounds enhanced pumping in both sexes **(Supplementary Fig. 2a),** indicating that ADIOL acts independently of biological sex.

Prior work showed that CR promotes learning and memory in *C. elegans* via reductions in KynA (10). While both NMDAR-dependent and independent learning paradigms exist, the benefits of reduced KynA were specific to NMDAR-dependent

learning (10). *mxl-3* mutants are a well-established CR model. Starvation represses *mxl-3* expression, which leads to increased autophagy (43). These mutants exhibit reduced KynA levels, as determined by biochemical assays, even when well-fed (10). They also show elevated pharyngeal pumping, dependent on the same signaling components required for the increased pumping observed in KynA-deficient *nkat-1* mutants **(Supplementary Fig. 2b),** as well as enhanced learning **(Fig. 1e)** (10). We found that the learning enhancement in *mxl-3* mutants is entirely dependent on the presence of *nhr-91* and *nhr-131* **(Fig. 1e)**. Consistent with prior data, *nhr-91* mutants show near-WT learning, while *nhr-131* mutants have significant deficits (9). These results suggest that ADIOL engagement of *nhr-91* is not required for baseline learning but is essential for learning enhancement under CR conditions recapitulated by *mxl-3* mutants. The baseline learning deficits of *nhr-131* mutants likely reflect its broader regulatory role in baseline learning, beyond influencing the production of ADIOL.

Similarly, *daf-2* (insulin receptor-deficient) and *rict-1* (mTOR pathway-deficient) mutants also exhibit reduced KynA levels and enhanced learning (10). Losses of *nhr-91* and *nhr-131* partially suppressed learning enhancement in *daf-2* mutants (**Fig. 1f**), whereas loss of *nhr-91* had no effect on the learning phenotype of *rict-1* mutants (**Supplementary Fig. 2c**). These findings support the idea that ADIOL plays a role in conditions of CR to increase learning capacity. They also reveal the complexity and diversity of the mechanisms involved in linking CR to mechanisms of learning and memory.

ADIOL levels increase under fasting and CR conditions through the upregulation of *CYP11A1*, *CYP17A1* and *17-βHSDs* orthologs

ADIOL is synthesized from cholesterol via a well-characterized enzymatic cascade: CYP11A1 converts cholesterol to pregnenolone (PREG); CYP17A1 transforms PREG into dehydroepiandrosterone (DHEA); and 17β-hydroxysteroid dehydrogenases (17β-HSDs) convert DHEA to ADIOL **(Fig. 2a)**. Prior work showed that the synthetic compound F17 increases ADIOL levels in *C. elegans* by activating NHR-131, which upregulates multiple *CYP17A1* and *17β-HSD* homologs **(Fig. 2a)** (9). To understand how ADIOL levels rise during fasting or in CR models, we analyzed the expression of these NHR-131-dependent, F17-upregulated genes after 2 hours of fasting and in *daf-2*, *mxl-3*, and *rict-1* mutants using RT-qPCR. We also included *cyp-44A1*, the homolog

of *CYP11A1*, which catalyzes the first step in the pathway, as its upregulation, though not induced by F17, could contribute to fasting-induced ADIOL synthesis.

A subset of these genes was upregulated after 2 hours of fasting and in *daf-2* mutants. Specifically, fasting induced expression of *cyp-44A1* (*CYP11A1*), *cyp-33C2* and *cyp-33C5* (*CYP17A1* homologs), and *F12E12.11* (*17β-HSD* homolog), most of which were also upregulated in *daf-2* mutants **(Fig. 2b, Supplementary Fig. 3)**. Surprisingly, *mxl-3* mutants did not show similar upregulation of these biosynthetic genes (**Fig. 2b)**, suggesting that in this model, ADIOL production or activity may be regulated by alternative mechanisms. To explore this possibility, we assessed expression of *nhr-91*, whose upregulation could amplify ADIOL signaling. Supporting this hypothesis, RT-qPCR analysis revealed elevated *nhr-91* expression in both *daf-2* and *mxl-3* mutants **(Fig. 2c)**, indicating that enhanced receptor expression may enhance ADIOL signaling.

We reasoned that if these biosynthetic genes mediate ADIOL production, their loss should mimic the effects of impaired ADIOL signaling. To test this, we examined post-fast pharyngeal pumping, a behavior known to require ADIOL and *nhr-91* **(Fig. 1)**. *cyp-44A1* mutants failed to elevate pharyngeal pumping following refeeding, while *cyp-13A4* and *F12E12.11* mutants showed only partial responses **(Fig. 2d)**. Similarly, RNAi knockdown of *cyp-33C2* and *cyp-33C5* (*CYP17A1* homologs) reduced post-fasting pumping **(Fig. 2e)**. These partial requirements likely reflect enzymatic redundancy, with multiple enzymes capable of catalyzing each step.

Together, these findings support a model in which fasting and CR enhance ADIOL production through upregulation of key biosynthetic genes, *cyp-44A1*, *cyp-33C2/5*, and *F12E12.11* **(Supplementary Fig. 3)**. In some contexts, increased expression of the ADIOL receptor *nhr-91* may also lead to elevated ADIOL signaling.

ADIOL promotes neuronal healthspan during aging through KynA reduction

A previous study demonstrated that ADIOL enhances learning and memory in aged animals by lowering KynA levels (11). However, whether ADIOL is required to maintain normal learning capacity throughout aging remains unknown. To address this, we examined learning capacity in *nhr-91* and *nhr-131* mutants across aging. While wild-type animals exhibit age-associated declines in learning, *nhr-91* mutants, which are

unable to respond to ADIOL, showed a markedly earlier and more pronounced decline (**Fig. 3a)**. Similarly, *nhr-131* mutants, which lack ADIOL biosynthesis, displayed severe impairments from early adulthood **(Fig. 3a)**.

Given that pharyngeal pumping is another established healthspan readout, we assessed this behavior in *nhr-91* and *nhr-131* mutants during aging. Despite elevated basal pumping in day 1 adults, both mutants exhibited accelerated declines in pharyngeal pumping compared to wild-type animals **(Fig. 3b)**. The reasons for the elevated basal pumping of these animals at the onset of adulthood are currently unknown. To test whether ADIOL's effects on pumping persist with age, we treated wild-type animals with ADIOL from the L4 stage onward. As expected, pharyngeal pumping declined with age in untreated animals, while ADIOL treatment blunted this decline **(Fig. 3c)**. To determine whether administration of ADIOL once the decline has begun is also effective, we treated day 4 adult animals with either the standard or a tenfold higher ADIOL dose and measured pumping on day 5. While the standard dose had no effect, the higher dose restored pumping to levels comparable to those seen with lifelong treatment (**Fig. 3d)**. Day 5 animals were previously demonstrated to have significantly elevated levels of KynA (11), providing a potential rationale as to why elevated doses of ADIOL are needed to elicit an increase in pharyngeal pumping.

To determine whether ADIOL's effects on pumping remain dependent on RIM neuron in aged animals, we examined *nhr-91*-deficient animals in which *nhr-91 was* specifically expressed in RIM or RIC neurons. Only RIM-specific reconstitution restored the ability of ADIOL to enhance pharyngeal pumping in day 5 adults, confirming the continued importance of this neuronal locus **(Fig. 3e)**.

To assess other indicators of healthspan, we next assessed mobility by measuring thrashing, the swimming movement of worms in liquid. As expected, thrashing declined with age **(Fig. 3f)**. ADIOL treatment from the L4 stage increased thrashing in day 1 adults, but its effects at later ages were modest and potentially obscured by the high variability of thrashing rate in the absence of treatment **(Fig. 3f)**. To better assess age-related effects, we repeated the experiment without FUDR and using a tenfold higher ADIOL concentration. Under these conditions, ADIOL robustly enhanced thrashing in aged animals **(Supplementary Fig. 4a)**. However, in the absence of FUDR and ADIOL, we observed an unexpected increase in thrashing rate of day 5

wild-type animals, coincident with termination of the egg-laying period **(Supplementary Fig. 4a)**. The basis for this increase is unclear.

We next tested whether ADIOL's effects on thrashing also require NHR-91 in RIM neurons. As with pharyngeal pumping, ADIOL enhanced thrashing only when NHR-91 was reconstituted in RIM neurons **(Fig. 3g)**. We next asked whether ADIOL's effect on thrashing depends on KynA. *nkat-1* mutants (low KynA) (9,40) exhibited elevated thrashing on both day 1 and day 5, while *kmo-1* mutants (high KynA) (9,40) showed normal thrashing **(Fig. 3h; Supplementary Fig. 1a)**. Consistent with a KynA-dependent mechanism, ADIOL failed to further enhance thrashing in aged *nkat-1* mutants **(Supplementary Fig. 4b, Fig. 3i)**.

We also evaluated whether ADIOL influences other aging-related phenotypes. ADIOL-treated animals showed modestly increased resistance to osmotic stress (NaCl) at several time points during aging **(Supplementary Fig. 4c)**. In contrast, chemotaxis to benzaldehyde was unaffected by ADIOL at any age **(Supplementary Fig. 4d)**. These data indicate that ADIOL enhances multiple, but not all, indicators of healthspan.

Together, these findings show that loss of ADIOL signaling via NHR-91 accelerates decline in multiple healthspan indicators, including learning, pharyngeal pumping, and mobility. Conversely, exogenous ADIOL administration mitigates these declines during aging through a mechanism that is mimicked by KynA depletion.

ADIOL suppresses the proteostatic stress induced by the Alzheimer's-associated APOE4 variant

Modulation of KP metabolites is increasingly recognized as a potential therapeutic strategy for neurodegenerative diseases (24,30). To explore whether ADIOL confers protective effects in a disease context, we tested its impact in a *C. elegans* model expressing the human Alzheimer's-associated APOE4 variant.

Previous studies have shown that APOE4 expression in *C. elegans* diminishes thermotolerance and elevates expression of a *hsp-16.2p::GFP*, a stress-activated reporter, primarily in body wall muscle (44). In thermotolerance assays, ADIOL had no effect in wild-type animals but significantly rescued the reduced heat stress resistance of APOE4 transgenics, restoring their thermotolerance to wild-type levels (**Fig. 4a)**. Furthermore, chronic exposure to high concentrations of ADIOL from the embryonic

stage led to a marked suppression of *hsp-16.2p*::*GFP* expression in the APOE4 model, with ~77% of animals showing decreased reporter activity **(Fig. 4b–f)**. ADIOL treatment did not alter *hsp-16.2p*::*GFP* expression in the wild-type background (**Supplementary Fig. 5)**.

The ability of ADIOL to restore thermotolerance and suppress stress reporter activation in the APOE4 model was comparable to that observed following activation of hypoxia-inducible factor-1 (HIF-1) (44), suggesting a robust protective effect against APOE4-induced stress.

The beneficial effects of ADIOL on healthspan are not merely a result of lifespan extension

An important question raised by these findings was whether ADIOL's healthspan benefits simply reflect changes in lifespan. Animals lacking the ADIOL receptor (*nhr-91* mutants) showed a modest reduction in mean lifespan (approximately one day shorter than wild-type animals) while *nhr-131* mutants, which likely lack biosynthesis of multiple steroid hormones including ADIOL, exhibited a more pronounced decrease **(Fig. 5a)**. However, ADIOL treatment did not extend the lifespan of wild-type animals **(Fig. 5b**). Furthermore, CR extended the lifespan of *nhr-91* mutants, and loss of *nhr-91* had no effect on the extended lifespans of long-lived *daf-2*, *mxl-3*, or *eat-2* mutants **(Fig. 5c–f)**.

These findings demonstrate that ADIOL's healthspan-promoting effects are not secondary to changes in lifespan. This conclusion is further supported by previous studies showing that reductions in KynA levels do not alter lifespan (10).

DISCUSSION

Our results indicate that ADIOL biosynthesis is enhanced under fasting and CR conditions, and that ADIOL signaling through the *C. elegans* homolog of estrogen receptor β, NHR-91, mediates several neural healthspan benefits associated with fasting and CR. ADIOL's effects on pharyngeal pumping, learning capacity, and thrashing, all indicators of healthspan, are dependent on NHR-91 activity in RIM neurons, a primary site of KynA production. Consistent with the KynA-lowering action of ADIOL, fasting/CR reduces KynA levels (10), and animals deficient in KynA exhibit

improved performance in the same healthspan indicators. While increasing ADIOL levels promotes healthspan during aging, loss of *nhr-91* accelerates age-associated decline in the specific indicators of healthspan tested. Together, these findings provide the first evidence that the steroid hormone ADIOL mediates key neural benefits of fasting and CR.

Supporting the notion that ADIOL biosynthesis is nutritionally regulated, several genes predicted to encode enzymes involved in its synthesis (homologs of *CYP11A1*, *CYP17A1*, and *17β-HSDs*) are upregulated following short-term fasting or in genetic models that mimic aspects of CR (**Fig. 2**). These enzymes convert cholesterol to ADIOL via pregnenolone (PREG) and DHEA (3).

While the link between fasting/CR and ADIOL production is a novel insight, prior studies in other species are consistent with our findings. Plasma DHEA levels increase during fasting in male zebra finches and in the lizard *Anolis sagrei* (45,46), and in rodents, fasting induces hepatic CYP17A1 expression and elevates DHEA levels via PGC-1α activation (47,48). In parallel, prolonged CR in mice increases expression of estrogen receptors, including ERβ (49), and in humans, CR reduces circulating kynurenine, the precursor of KynA, within just two weeks (50). However, whether ADIOL levels are modulated by fasting/CR in mammals remains unknown.

Importantly, not all CR models depend on ADIOL to improve learning capacity **(Fig. 1e–f, Supplementary Fig. 2c)**, suggesting that while ADIOL is a key contributor, it is not the sole mediator of CR-induced benefits. We previously found that fasting and CR models regulate *kmo-1*, encoding kynurenine monooxygenase-1, which competes with KATs for the substrate kynurenine (10). Thus, KMO-1 activity may influence KynA production independently of ADIOL, highlighting multiple regulatory routes by which fasting/CR can lower KynA and improve neural function.

Prompted by ADIOL's ability to improve healthspan, we explored its effects in a neurodegenerative disease model. Neurodegenerative diseases such as Alzheimer's remain incurable and are major contributors to age-related morbidity. In *C. elegans* expressing the human APOE4 variant, associated with proteostatic stress and elevated *hsp-16.2p*::*GFP* expression, ADIOL treatment restored thermotolerance and suppressed stress reporter activation, effects comparable to those achieved by HIF-1 activation **(Fig. 4)**.

Importantly, ADIOL did not extend lifespan in wild-type animals (**Fig. 5**), and its receptor mutant, *nhr-91*, showed only a modest lifespan reduction. Furthermore, *nhr-91* was not required for lifespan extension in long-lived mutants such as *daf-2*, *mxl-3*, or *eat-2*. These findings indicate that ADIOL's healthspan-promoting effects are not indirect consequences of lifespan extension. This is consistent with prior observations that KynA depletion does not alter lifespan (10). This distinction is especially relevant given the growing interest in closing the lifespan-healthspan gap (1).

What molecular mechanisms underlie the ADIOL–NHR-91/ERβ–KynA axis in promoting neural resilience? While the full picture is not yet known, KynA's signaling roles offer a plausible mechanistic framework. In mammals, KynA is a known agonist of the aryl hydrocarbon receptor (AhR) and GPR35, and an antagonist of several glutamate receptors, including NMDARs, which are critical for synaptic plasticity, learning, and memory (51-53). We previously showed that the behavioral benefits of KynA reduction in *C. elegans* depend on enhanced activity of specific neurons in an NMDAR-dependent manner (10). The precise means by which KynA modulates NMDAR-dependent neural activity in *C. elegans* remains to be determined.

In the context of Alzheimer's disease, activation of the kynurenine pathway contributes to disrupted proteostasis, inflammation, glial dysfunction, and impaired neuronal metabolism (54-56). Astrocyte-derived lactate, a key neuronal fuel, is regulated by the transcription factor HIF-1α and its cofactor ARNT1 (55,56). Notably, Kyn and KynA both activate AhR, which competes with HIF-1α for ARNT1. A recent landmark study showed that increased Kyn levels in Alzheimer's models activate AhR, sequestering ARNT1 and impairing lactate production. Blocking kynurenine pathway activation by inhibiting one of the enzymes that catalyzes import of tryptophan into the kynurenine pathway reversed these metabolic defects and restored memory and synaptic function (56).

Together, our findings show that ADIOL biosynthesis pathway is nutritionally sensitive and that this overlooked steroid hormone improves multiple indicators of neural healthspan and resilience. The results also point to KynA reducing effects of ADIOL as the likely molecular explanation. In light of these findings, ADIOL emerges as a promising mimetic of dietary restriction effects on healthspan, highlighting its potential as a therapeutic strategy for age-related neurodegenerative conditions.

MATERIALS AND METHODS

Strains and maintenance

Strains used in this study are listed in **Supplementary Table 1**. Plasmid constructs were generated by standard PCR amplification from *C. elegans* genomic DNA or cDNA and assembled using NEBuilder HiFi DNA Assembly (New England Biolabs). Transgenic extrachromosomal arrays included Ex[*cex-1p::nhr-91,unc-122::GFP*], which used a 0.9 kb region upstream of the ATG start codon of *cex-1* as promoter and included *unc-122::GFP* as a coinjection marker. Ex[*tbh-1p::nhr-91cDNA::SL2::GFP*] used 3,455 bp upstream of the ATG of *tbh-1* as promoter and contained the full *nhr-91* cDNA followed by a bicistronic SL2::GFP reporter. The 3′ untranslated region (UTR) of *unc-54* was used for all constructs to ensure proper transcript processing. Transgenic animals carrying non-integrated extrachromosomal arrays were generated by microinjecting expression plasmids into the gonad arm at final concentrations ranging from 5 to 50 ng/µL. Double mutants were obtained through standard genetic crosses between males and hermaphrodites.

Unless otherwise specified, *C. elegans* were maintained at 20 °C on 6-cm NGM agar plates seeded with *Escherichia coli* OP50, following established protocols (57).

RNAi

RNAi clones targeting *cyp-33C2* and *cyp-33C5* (Ahringer library) (58) were used for gene knockdown experiments. The empty vector L4440 was used as a negative control, and the *nkat-1* RNAi clone was included as a positive control. *E. coli* HT115 strains containing the respective RNAi plasmids were grown overnight at 37 °C in 5 mL of LB supplemented with 100 µg/mL carbenicillin. Cultures were then diluted 1:40 into 5 mL of fresh LB with 100 µg/mL carbenicillin and grown at 37 °C with shaking until reaching an OD_{600} of 0.4-0.6. Double-stranded RNA production was induced by adding 1 mM IPTG and incubating for 4 h at 37 °C. To spike the induction, cultures were supplemented with an additional 100 µg/mL carbenicillin and 1 mM IPTG. A total of 250 µL of induced culture was seeded onto 6-cm NGM plates containing 100 µg/mL carbenicillin and 1 mM IPTG. Plates were incubated overnight at room temperature to allow bacterial lawn formation. Synchronized L1 animals were then transferred onto the RNAi plates and maintained at 20 °C until the L4 stage for further experiments.

Pharmacological treatments

The pharmacological treatments used in this study were F17 (custom synthesis, TimTec) and 5-androstene-3β,17β-diol (ADIOL) (Steraloids). Both compounds were dissolved in DMSO, which served as the vehicle. F17 was applied at a final concentration of 2.5 μM, and ADIOL was administered at a final concentration of 10 nM, with a subset of experiments including a tenfold higher dose (10X; 100 nM) to assess dose-dependent effects. Concentrations were calculated based on the total NGM volume per plate and were mixed with *E. coli* OP50 prior to seeding. Unless otherwise specified, treatments were initiated at the L4 larval stage.

2-h fasting

Fasting was conducted by collecting animals in 1 mL of S-basal + 0.05% PEG-8000 and washing them three times with the same solution. After washing, worms were rotated for 2 hours in the same buffer. For pharyngeal pumping assessment, animals were transferred to plates seeded with *E. coli* OP50 and allowed to acclimate for at least 5 minutes before counting.

Pharyngeal pumping

Pharyngeal pumping was assessed by counting the number of contractions of the posterior pharyngeal bulb over a 10-second period, as previously described (40). The assay was performed on 20 L4 or day 1 adult animals per condition. Animals were age-synchronized using standard hypochlorite treatment of gravid hermaphrodites to isolate eggs, which were allowed to hatch overnight in S-basal supplemented with 0.05% PEG-8000. Approximately 150 synchronized L1 larvae per condition were transferred onto 6-cm NGM plates and incubated at 20 °C until they reached the developmental stage required for each assay. For aging studies, day 1 adults were placed on plates containing 50 μM FUDR (RPI) and moved to fresh FUDR plates every other day until evaluation.

Short-term associative learning

Short-term associative learning was performed as previously described (9) with minor modifications. Animals were age-synchronized via bleaching and allowed to hatch overnight in S-basal supplemented with 0.05% PEG-8000. Approximately 250 L1

larvae per condition and replicate were transferred onto 6-cm NGM plates and incubated at 20 °C until they reached the appropriate developmental stage for the assay. For aging studies, day 1 adults were placed on plates containing 50 µM FUDR (RPI) and moved to fresh FUDR plates every other day until evaluation. The day before the experiment, animals were transferred to plates dried for 2 h in a laminar flow hood. On the day of the experiment, conditioned animals were exposed to butanone by streaking 5 µL of a 10% (v/v) butanone solution in ethanol on the underside of the lid of a 6-cm plate, and incubated in a humidified chamber for 60 min at 20 °C. After conditioning, animals were washed off the plate using 1 mL of S-basal + 0.05% PEG-8000 and transferred into 1.5-mL tubes to settle for approximately 2 minutes. A 20 µL aliquot of the settled pellet was then placed at the origin of a 10-cm chemotaxis plate containing butanone and ethanol. Chemotaxis plates were prepared by spotting 2 µL of 2% sodium azide onto the locations designated for butanone or ethanol. Plates were left for approximately 10 minutes to allow the sodium azide to absorb into the agar. Subsequently, 2 µL of ethanol or 10% butanone (v/v) were added to the respective spots on each plate. The same procedure was followed for non-conditioned control animals. Excess moisture at the deposition site was gently absorbed using a folded tissue to release animals onto the plate for chemotaxis. After 1 h of chemotaxis at 20 °C, plates were transferred to a 4 °C cold room to immobilize the animals until scoring.

The learning index was calculated as the difference between the chemotaxis index (for butanone-conditioned animals) and the naive index (for non-conditioned animals), where each index corresponds to [(number of animals in butanone − number of animals in ethanol) / total number of animals not remaining at the origin].

Thrashing

Thrashing was assessed by counting the number of body bends made by each animal in 20 µL of M9 buffer over a 30-second period. The assay was performed on at least 20 day 1 adult adults per condition. Animals were age-synchronized via standard hypochlorite treatment of gravid hermaphrodites to isolate eggs, which were allowed to hatch overnight in S-basal supplemented with 0.05% PEG-8000. Approximately 150 synchronized L1 larvae per condition were transferred to 6-cm NGM plates and incubated at 20 °C until they reached the developmental stage required for each

assay. For aging studies, day 1 adults were either transferred to plates containing 50 μM FUDR (RPI) and moved to fresh FUDR plates every other day until evaluation, or transferred daily to fresh plates without FUDR using a platinum wire.

Osmotic stress resistance assay

For the osmotic stress resistance assay, 30 synchronized animals at day 1, 5, or 10 of adulthood were manually transferred using a platinum wire to NGM plates containing high salt concentration (400 mM NaCl) and seeded with *E. coli* OP50. Plates were incubated at 20 °C, and survival was assessed after 48 hours by gently prodding with a platinum wire. Animals that failed to respond were scored as dead. Treatment with DMSO (vehicle) or 10 nM ADIOL was initiated at the L4 stage and discontinued at the time of transfer to the osmotic stress plates. To assess animals on days 5 and 10 of adulthood, they were transferred daily to fresh FUDR-free plates using a platinum wire until reaching the corresponding stages.

Benzaldehyde chemotaxis

The benzaldehyde chemotaxis assay was performed as previously described (9). The benzaldehyde chemotaxis index was calculated as (number of animals in benzaldehyde - number of animals in ethanol)/(total number of animals). To prepare the animals for the assay, gravid hermaphrodites were age-synchronized via standard hypochlorite treatment to isolate eggs, which were allowed to hatch overnight in S-basal supplemented with 0.05% PEG-8000. Approximately 150 synchronized L1 larvae per condition were transferred to 6-cm NGM plates and incubated at 20 °C until they reached the developmental stage required for each assay. For aging studies, day 1 adults were placed on plates containing 50 μM FUDR (RPI) and moved to fresh FUDR plates every other day until evaluation.

Heat resistance assay

For the heat resistance assay, animals were maintained under well-fed conditions for at least two generations prior to the experiment. Treatment with DMSO (vehicle) or 100 nM ADIOL (10X) started at the embryo stage ($n \geq 50$). Upon reaching the L4 stage, animals were transferred to fresh NGM plates seeded with *E. coli* OP50 and incubated

at 28 °C. Survival was monitored every 24 hours by gently prodding with a platinum wire. Animals that failed to respond were scored as dead.

Confocal imaging

Animals of different genotypes exposed to DMSO (vehicle), 10 nM ADIOL, or 100 nM ADIOL from the embryonic stage were randomly selected upon reaching the day 1 adult stage and anesthetized with 10 mM sodium azide (Sigma-Aldrich) in M9 buffer. Worms were then aligned on 2% agarose pads on microscope slides, and images were acquired using a Leica TCS SPE confocal microscope and the 20X (low magnification) and 63X (high magnification) objective lenses. Identical acquisition settings were used for all samples.

Lifespan

For lifespan assessment, animals synchronized by egg-laying instead of bleaching were grown until day 1 of adulthood on 6-cm NGM plates seeded with *E. coli* OP50. From that day onward, survival was monitored daily until no live adults remained. Animals were scored as dead if they failed to respond when gently prodded with a platinum wire. In all assays, animals were transferred to plates containing 50 μM FUDR from day 1 to day 8 of adulthood, being moved to fresh plates every other day. The only exception was the CR experiment, where *ad libitum* (AL) fed animals were transferred every other day to fresh plates seeded with *E. coli* OP50 using a platinum wire, while CR animals were transferred every other day starting from day 3 of adulthood to NGM plates without OP50, relying solely on the small amount of bacteria carried over with the platinum wire during transfer.

RT-qPCR

Approximately 300 synchronized L1 larvae were transferred onto 6-cm NGM plates per replicate and allowed to develop to the L4 stage. Worms treated with DMSO (vehicle) or F17 were exposed to the compounds overnight prior to reaching the L4 stage. Total RNA was extracted from these animals using TRIzol reagent and purified with the Direct-zol RNA Miniprep Kit (Zymo Research), including on-column DNase treatment. First-strand cDNA was synthesized using the ProtoScript II First Strand cDNA Synthesis Kit (New England Biolabs) with random primers.

Quantitative PCR was performed using the SsoAdvanced Universal SYBR Green Supermix (Bio-Rad) on a C100 Touch™ Thermal Cycler CFX384™ Real-Time System (Bio-Rad), in 384-well plates. The reactions (10 µL final volume) contained 5 µL of SYBR Green Supermix, 0.5 µL of gene-specific primers (5 µM), 1 µL of cDNA (diluted 1:4), and 3.5 µL of nuclease-free water.

Cycling conditions followed a two-step protocol: initial denaturation at 95 °C for 3 min, followed by 40 cycles of 95 °C for 10 s and 60 °C for 30 s, ending with a melting curve analysis. Each sample was analyzed in technical triplicates, and appropriate negative controls were included. Threshold cycle (Ct) values were obtained using CFX Manager v3.1 software (Bio-Rad). Gene expression was normalized to the reference gene *tba-1*. Relative expression levels were calculated using the $2^{-\Delta\Delta Ct}$ method. Primer sequences are provided in **Supplementary Table 2**.

Data visualization and statistics

Statistical analyses and graphical representations were performed using StataSE v12 (StataCorp LP, College Station, TX, USA) and GraphPad Prism 8.0.2 (GraphPad Software, San Diego, CA, USA). Normality was assessed using the Shapiro-Wilk test, except for feeding and thrashing data, for which the D'Agostino test was used due to the high number of repeated values. To enhance clarity, the choice between reporting the mean +/- standard deviation (SD) or the median +/- interquartile range (IQR), as well as the specific statistical test used, is indicated in each figure legend. The significance level (α) was set at 0.05, except for the log-rank test, where it was adjusted to 0.01 to reduce the risk of type I errors (false positives).

DECLARATIONS

Author contributions

Conceptualization, K.A., G.A.L., and A.G.-H.; methodology, A.G.-H., S.Y., G.A.L., and W.I.J.; formal analysis, A.G.-H. and W.I.J.; investigation, A.G.-H., S.Y., S.K., W.I.J., A.Q.L., R.R.P.; resources, K.A. and D.K.M.; data curation, A.G.-H. and W.I.J.; validation, S.Y., S.K., and A.G.-H.; writing – original draft preparation A.G.-H., K.A.; writing – review & editing, K.A., A.G.-H., G.A.L., S.Y., S.K.; visualization, A.G.-H. and W.I.J.; supervision, K.A. and D.K.M.; funding acquisition, K.A. and D.K.M.

Competing interests

The authors declare no competing interests.

Acknowledgements

Some strains were provided by the Caenorhabditis Genetics Center (CGC), which is funded by NIH Office of Research Infrastructure Programs (P40 OD010440). This work was supported by NIH grants R01AG046400 and RF1AG068194 to K.A.

REFERENCES

1. Khan M, Al Saud H, Sierra F, Perez V, Greene W, Al Asiry S, Pathai S, Torres M. Global Healthspan Summit 2023: closing the gap between healthspan and lifespan. *Nat Aging*. 2024;4(4):445-448. doi: 10.1038/s43587-024-00593-4.
2. Cole TJ, Short KL, Hooper SB. The science of steroids. *Semin Fetal Neonatal Med*. 2019;24(3):170-175. doi: 10.1016/j.siny.2019.05.005.
3. Luu-The V. Assessment of steroidogenesis and steroidogenic enzyme functions. *J Steroid Biochem Mol Biol*. 2013;137:176-82. doi: 10.1016/j.jsbmb.2013.05.017.
4. Coffey DS. Androgen action and the sex accessory tissues. In: Knobil E, Neill J, editors. The Physiology of Reproduction. New York: Raven Press; 1988. p. 1081–1119.
5. Kuiper GG, Carlsson B, Grandien K, Enmark E, Häggblad J, Nilsson S, Gustafsson JA. Comparison of the ligand binding specificity and transcript tissue distribution of estrogen receptors alpha and beta. *Endocrinology*. 1997;138(3):863-70. doi: 10.1210/endo.138.3.4979.
6. Manolagas SC, Anderson DC, Lindsay R. Adrenal steroids and the development of osteoporosis in oophorectomised women. *Lancet Lond Engl*. 1979;2(8143):597–600.
7. Li ZM, Kannan K. Determination of 19 Steroid Hormones in Human Serum and Urine Using Liquid Chromatography-Tandem Mass Spectrometry. *Toxics*. 2022;10(11):687.

8. Saijo K, Collier JG, Li AC, Katzenellenbogen JA, Glass CK. An ADIOL-ERβ-CtBP transrepression pathway negatively regulates microglia-mediated inflammation. *Cell*. 2011;145(4):584-95. doi: 10.1016/j.cell.2011.03.050.

9. Lemieux GA, Yoo S, Lin L, Vohra M, Ashrafi K. The steroid hormone ADIOL promotes learning by reducing neural kynurenic acid levels. *Genes Dev*. 2023;37(21-24):998-1016. doi: 10.1101/gad.350745.123.

10. Vohra M, Lemieux GA, Lin L, Ashrafi K. The beneficial effects of dietary restriction on learning are distinct from its effects on longevity and mediated by depletion of a neuroinhibitory metabolite. *PLoS Biol*. 2017;15(8):e2002032. doi: 10.1371/journal.pbio.2002032.

11. Vohra M, Lemieux GA, Lin L, Ashrafi K. Kynurenic acid accumulation underlies learning and memory impairment associated with aging. *Genes Dev*. 2018;32(1):14-19. doi: 10.1101/gad.307918.117.

12. Arey RN, Stein GM, Kaletsky R, Kauffman A, Murphy CT. Activation of $G_{\alpha q}$ Signaling Enhances Memory Consolidation and Slows Cognitive Decline. *Neuron*. 2018;98(3):562-574.e5. doi: 10.1016/j.neuron.2018.03.039.

13. Lakhina V, Arey RN, Kaletsky R, Kauffman A, Stein G, Keyes W, Xu D, Murphy CT. Genome-wide functional analysis of CREB/long-term memory-dependent transcription reveals distinct basal and memory gene expression programs. *Neuron*. 2015;85(2):330-45. doi: 10.1016/j.neuron.2014.12.029.

14. Torayama I, Ishihara T, Katsura I. *Caenorhabditis elegans* integrates the signals of butanone and food to enhance chemotaxis to butanone. *J Neurosci*. 2007;27(4):741-50. doi: 10.1523/JNEUROSCI.4312-06.2007.

15. Kauffman AL, Ashraf JM, Corces-Zimmerman MR, Landis JN, Murphy CT. Insulin signaling and dietary restriction differentially influence the decline of learning and memory with age. *PLoS Biol*. 2010;8(5):e1000372. doi: 10.1371/journal.pbio.1000372.

16. Potter MC, Elmer GI, Bergeron R, Albuquerque EX, Guidetti P, Wu HQ, Schwarcz R. Reduction of endogenous kynurenic acid formation enhances extracellular

glutamate, hippocampal plasticity, and cognitive behavior. *Neuropsychopharmacology*. 2010;35(8):1734-42. doi: 10.1038/npp.2010.39.

17. Moroni F, Russi P, Carlá V, Lombardi G. Kynurenic acid is present in the rat brain and its content increases during development and aging processes. *Neurosci Lett*. 1988;94(1-2):145-50. doi: 10.1016/0304-3940(88)90285-6.

18. Alexander KS, Wu HQ, Schwarcz R, Bruno JP. Acute elevations of brain kynurenic acid impair cognitive flexibility: normalization by the alpha7 positive modulator galantamine. *Psychopharmacology (Berl)*. 2012;220(3):627-37. doi: 10.1007/s00213-011-2539-2.

19. Chess AC, Landers AM, Bucci DJ. L-kynurenine treatment alters contextual fear conditioning and context discrimination but not cue-specific fear conditioning. *Behav Brain Res*. 2009;201(2):325-31. doi: 10.1016/j.bbr.2009.03.013.

20. Chess AC, Simoni MK, Alling TE, Bucci DJ. Elevations of endogenous kynurenic acid produce spatial working memory deficits. *Schizophr Bull*. 2007;33(3):797-804. doi: 10.1093/schbul/sbl033.

21. Chess AC, Bucci DJ. Increased concentration of cerebral kynurenic acid alters stimulus processing and conditioned responding. *Behav Brain Res*. 2006;170(2):326-32. doi: 10.1016/j.bbr.2006.03.006.

22. DeAngeli NE, Todd TP, Chang SE, Yeh HH, Yeh PW, Bucci DJ. Exposure to Kynurenic Acid during Adolescence Increases Sign-Tracking and Impairs Long-Term Potentiation in Adulthood. *Front Behav Neurosci*. 2015;8:451. doi: 10.3389/fnbeh.2014.00451.

23. Gramsbergen JB, Schmidt W, Turski WA, Schwarcz R. Age-related changes in kynurenic acid production in rat brain. *Brain Res*. 1992;588(1):1-5. doi: 10.1016/0006-8993(92)91337-e.

24. Cervenka I, Agudelo LZ, Ruas JL. Kynurenines: Tryptophan's metabolites in exercise, inflammation, and mental health. *Science*. 2017;357(6349):eaaf9794. doi: 10.1126/science.aaf9794.

25. Schwarcz R, Bruno JP, Muchowski PJ, Wu HQ. Kynurenines in the mammalian brain: when physiology meets pathology. *Nat Rev Neurosci*. 2012;13(7):465-77. doi: 10.1038/nrn3257.

26. Schwarcz R, Stone TW. The kynurenine pathway and the brain: Challenges, controversies and promises. *Neuropharmacology*. 2017;112(Pt B):237-247. doi: 10.1016/j.neuropharm.2016.08.003.

27. Kolodziej LR, Paleolog EM, Williams RO. Kynurenine metabolism in health and disease. *Amino Acids*. 2011;41(5):1173-83. doi: 10.1007/s00726-010-0787-9.

28. Stone TW, Darlington LG. The kynurenine pathway as a therapeutic target in cognitive and neurodegenerative disorders. *Br J Pharmacol*. 2013;169(6):1211-27. doi: 10.1111/bph.12230.

29. Joisten N, Ruas JL, Braidy N, Guillemin GJ, Zimmer P. The kynurenine pathway in chronic diseases: a compensatory mechanism or a driving force? *Trends Mol Med*. 2021;27(10):946-954. doi: 10.1016/j.molmed.2021.07.006.

30. Johnson LA, Macauley SL. Alzheimer's and metabolism wed with IDO1. *Science*. 2024;385(6711):826-827. doi: 10.1126/science.adr5836.

31. Kaiser H, Parker E, Hamrick MW. Kynurenine signaling through the aryl hydrocarbon receptor: Implications for aging and healthspan. *Exp Gerontol*. 2020;130:110797. doi: 10.1016/j.exger.2019.110797.

32. Lustgarten MS, Fielding RA. Metabolites related to renal function, immune activation, and carbamylation are associated with muscle composition in older adults. *Exp Gerontol*. 2017;100:1-10. doi: 10.1016/j.exger.2017.10.003.

33. Kim BJ, Hamrick MW, Yoo HJ, Lee SH, Kim SJ, Koh JM, Isales CM. The Detrimental Effects of Kynurenine, a Tryptophan Metabolite, on Human Bone Metabolism. *J Clin Endocrinol Metab*. 2019;104(6):2334-2342. doi: 10.1210/jc.2018-02481.

34. Apalset EM, Gjesdal CG, Ueland PM, Øyen J, Meyer K, Midttun Ø, Eide GE, Tell GS. Interferon gamma (IFN-γ)-mediated inflammation and the kynurenine pathway in relation to risk of hip fractures: the Hordaland Health Study. *Osteoporos Int*. 2014;25(8):2067-75. doi: 10.1007/s00198-014-2720-7.

35. Zuo H, Ueland PM, Ulvik A, Eussen SJ, Vollset SE, Nygård O, Midttun Ø, Theofylaktopoulou D, Meyer K, Tell GS. Plasma Biomarkers of Inflammation, the Kynurenine Pathway, and Risks of All-Cause, Cancer, and Cardiovascular Disease Mortality: The Hordaland Health Study. *Am J Epidemiol*. 2016;183(4):249-58. doi: 10.1093/aje/kwv242.

36. Kaiser H, Yu K, Pandya C, Mendhe B, Isales CM, McGee-Lawrence ME, Johnson M, Fulzele S, Hamrick MW. Kynurenine, a Tryptophan Metabolite That Increases with Age, Induces Muscle Atrophy and Lipid Peroxidation. *Oxid Med Cell Longev*. 2019;2019:9894238. doi: 10.1155/2019/9894238.

37. Refaey ME, McGee-Lawrence ME, Fulzele S, Kennedy EJ, Bollag WB, Elsalanty M, Zhong Q, Ding KH, Bendzunas NG, Shi XM, Xu J, Hill WD, Johnson MH, Hunter M, Pierce JL, Yu K, Hamrick MW, Isales CM. Kynurenine, a Tryptophan Metabolite That Accumulates With Age, Induces Bone Loss. *J Bone Miner Res*. 2017;32(11):2182-2193. doi: 10.1002/jbmr.3224.

38. Keith SA, Amrit FR, Ratnappan R, Ghazi A. The *C. elegans* healthspan and stress-resistance assay toolkit. *Methods*. 2014;68(3):476-86. doi: 10.1016/j.ymeth.2014.04.003.

39. Lemieux GA, Liu J, Mayer N, Bainton RJ, Ashrafi K, Werb Z. A whole-organism screen identifies new regulators of fat storage. *Nat Chem Biol*. 2011;7(4):206-13. doi: 10.1038/nchembio.534.

40. Lemieux GA, Cunningham KA, Lin L, Mayer F, Werb Z, Ashrafi K. Kynurenic acid is a nutritional cue that enables behavioral plasticity. *Cell*. 2015;160(1-2):119-31. doi: 10.1016/j.cell.2014.12.028.

41. Kasuga H, Fukuyama M, Kitazawa A, Kontani K, Katada T. The microRNA miR-235 couples blast-cell quiescence to the nutritional state. *Nature*. 2013;497(7450):503-6. doi: 10.1038/nature12117.

42. Greer ER, Pérez CL, Van Gilst MR, Lee BH, Ashrafi K. Neural and molecular dissection of a *C. elegans* sensory circuit that regulates fat and feeding. *Cell Metab*. 2008;8(2):118-31. doi: 10.1016/j.cmet.2008.06.005.

43. O'Rourke EJ, Ruvkun G. MXL-3 and HLH-30 transcriptionally link lipolysis and autophagy to nutrient availability. *Nat Cell Biol*. 2013;15(6):668-76. doi: 10.1038/ncb2741.

44. Jiang WI, Cao Y, Xue Y, Ji Y, Winer BY, Chandra R, Zhang XF, Zhang M, Singhal NS, Pierce JT, Chen S, Ma DK. Suppressing APOE4-induced neural pathologies by targeting the VHL-HIF axis. *Proc Natl Acad Sci U S A*. 2025;122(5):e2417515122. doi: 10.1073/pnas.2417515122.

45. Fokidis HB, Prior NH, Soma KK. Fasting increases aggression and differentially modulates local and systemic steroid levels in male zebra finches. *Endocrinology*. 2013;154(11):4328-39. doi: 10.1210/en.2013-1171.

46. Himmelstein R, Spahija A, Fokidis HB. Evidence for fasting induced extra-adrenal steroidogenesis in the male brown anole, Anolis sagrei. *Comp Biochem Physiol B Biochem Mol Biol*. 2021;253:110544. doi: 10.1016/j.cbpb.2020.110544.

47. Grasfeder LL, Gaillard S, Hammes SR, Ilkayeva O, Newgard CB, Hochberg RB, Dwyer MA, Chang CY, McDonnell DP. Fasting-induced hepatic production of DHEA is regulated by PGC-1alpha, ERRalpha, and HNF4alpha. *Mol Endocrinol*. 2009;23(8):1171-82. doi: 10.1210/me.2009-0024.

48. Milona A, Massafra V, Vos H, Naik J, Artigas N, Paterson HAB, Bijsmans ITGW, Willemsen ECL, Ramos Pittol JM, Miguel-Aliaga I, Bosma P, Burgering BMT, Williamson C, Vernia S, Dhillo WS, van Mil SWC, Owen BM. Steroidogenic control of liver metabolism through a nuclear receptor-network. *Mol Metab*. 2019;30:221-229. doi: 10.1016/j.molmet.2019.09.007.

49. Słuczanowska-Głąbowska S, Laszczyńska M, Piotrowska K, Grabowska M, Grymuła K, Ratajczak MZ. Caloric restriction increases ratio of estrogen to androgen receptors expression in murine ovaries--potential therapeutic implications. *J Ovarian Res*. 2015;8:57. doi: 10.1186/s13048-015-0185-8.

50. Strasser B, Berger K, Fuchs D. Effects of a caloric restriction weight loss diet on tryptophan metabolism and inflammatory biomarkers in overweight adults. *Eur J Nutr*. 2015;54(1):101-7. doi: 10.1007/s00394-014-0690-3.

51. DiNatale BC, Murray IA, Schroeder JC, Flaveny CA, Lahoti TS, Laurenzana EM, Omiecinski CJ, Perdew GH. Kynurenic acid is a potent endogenous aryl hydrocarbon receptor ligand that synergistically induces interleukin-6 in the presence of inflammatory signaling. *Toxicol Sci*. 2010;115(1):89-97. doi: 10.1093/toxsci/kfq024.

52. Wang J, Simonavicius N, Wu X, Swaminath G, Reagan J, Tian H, Ling L. Kynurenic acid as a ligand for orphan G protein-coupled receptor GPR35. *J Biol Chem*. 2006;281(31):22021-22028. doi: 10.1074/jbc.M603503200.

53. Stone TW. Neuropharmacology of quinolinic and kynurenic acids. *Pharmacol Rev*. 1993;45(3):309-79.

54. Cortés Malagón EM, López Ornelas A, Olvera Gómez I, Bonilla Delgado J. The Kynurenine Pathway, Aryl Hydrocarbon Receptor, and Alzheimer's Disease. *Brain Sci*. 2024;14(9):950. doi: 10.3390/brainsci14090950.

55. Sharma VK, Singh TG, Prabhakar NK, Mannan A. Kynurenine Metabolism and Alzheimer's Disease: The Potential Targets and Approaches. *Neurochem Res*. 2022;47(6):1459-1476. doi: 10.1007/s11064-022-03546-8.

56. Minhas PS, Jones JR, Latif-Hernandez A, Sugiura Y, Durairaj AS, Wang Q, Mhatre SD, Uenaka T, Crapser J, Conley T, Ennerfelt H, Jung YJ, Liu L, Prasad P, Jenkins BC, Ay YA, Matrongolo M, Goodman R, Newmeyer T, Heard K, Kang A, Wilson EN, Yang T, Ullian EM, Serrano GE, Beach TG, Wernig M, Rabinowitz JD, Suematsu M, Longo FM, McReynolds MR, Gage FH, Andreasson KI. Restoring hippocampal glucose metabolism rescues cognition across Alzheimer's disease pathologies. *Science*. 2024;385(6711):eabm6131. doi: 10.1126/science.abm6131.

57. Brenner S. The genetics of *Caenorhabditis elegans*. *Genetics*. 1974;77(1):71-94. doi: 10.1093/genetics/77.1.71.

58. Kamath RS, Fraser AG, Dong Y, Poulin G, Durbin R, Gotta M, Kanapin A, Le Bot N, Moreno S, Sohrmann M, Welchman DP, Zipperlen P, Ahringer J. Systematic functional analysis of the *Caenorhabditis elegans* genome using RNAi. *Nature*. 2003;421(6920):231-7. doi: 10.1038/nature01278.

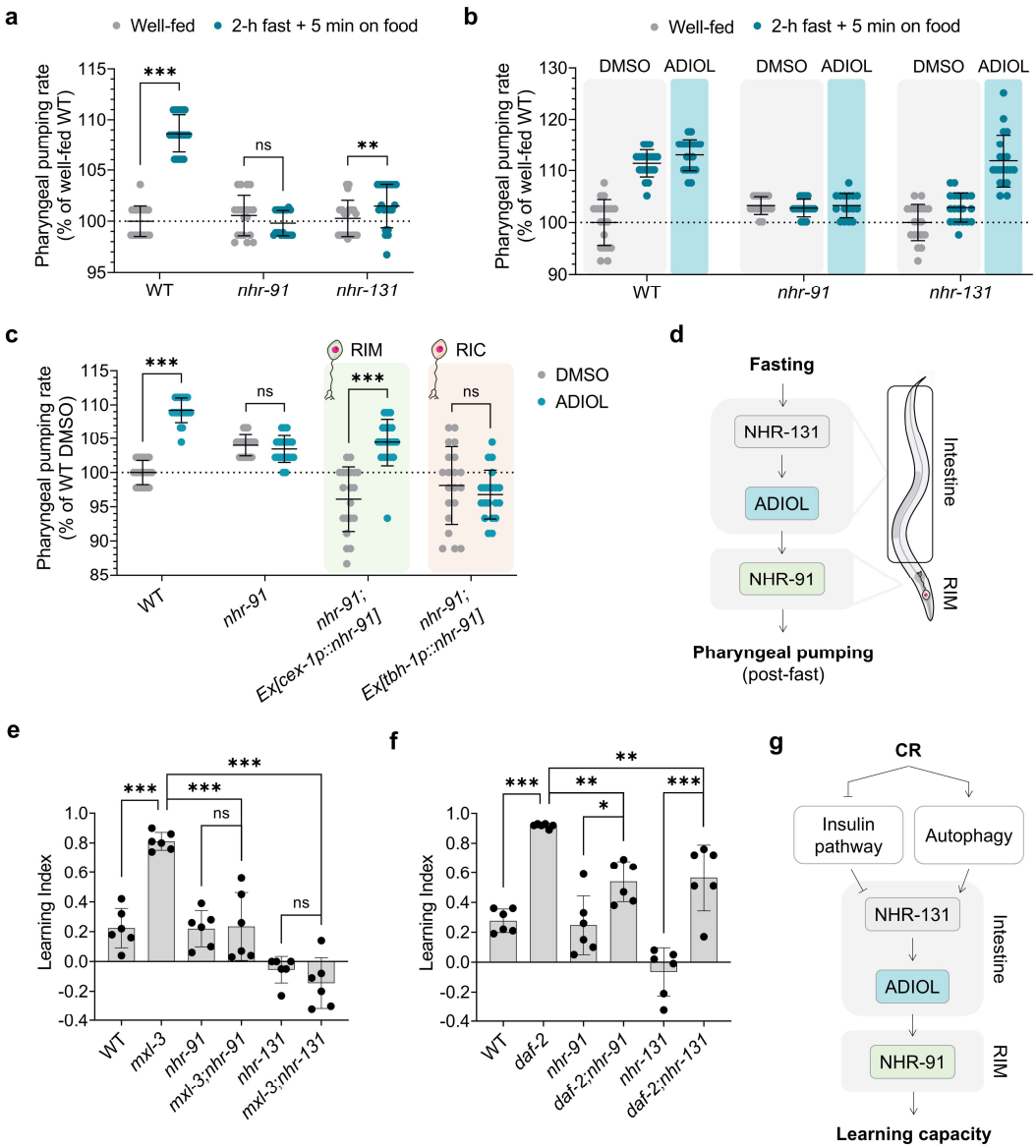

Figure 1. **ADIOL is required for the effects of nutrient limitation on pumping rate and learning capacity. (a and b)** Pharyngeal pumping rate in L4-stage animals under fed and post-fasting conditions. Animals were assessed for the number of pharyngeal pumps over 30 seconds in well-fed conditions and after a 2-hour fasting period followed by 5 minutes of re-exposure to food. Data are presented as the percentage of the pharyngeal pumping rate normalized to the mean of well-fed wild-type (WT) animals (n = 20 per condition). Error bars indicate the standard deviation (SD) of the proportion. **(a)** WT, *nhr-91*, and *nhr-131* animals were analyzed. Statistical analysis for the comparison between ADIOL-treated and DMSO-treated animals was performed using the t-test on raw data (***p < 0.001, **p < 0.01, ns: non-significant). **(b)** WT, *nhr-91*, and *nhr-131* animals treated with DMSO (vehicle) or 10 nM ADIOL from the L1 stage. **(c)** Pharyngeal pumping rate in day 1 adults of WT, *nhr-91*, *nhr-91*;Ex[*cex-1p::nhr-91*,*unc-122::GFP*], and *nhr-91*;Ex[*tbh-1p::nhr-91cDNA::sl2::GFP*] strains treated with DMSO (vehicle) or 10 nM ADIOL from the L4 stage. Data are presented as the percentage of

the pharyngeal pumping rate normalized to the mean of DMSO-treated WT animals (n = 20 per condition). Error bars indicate the standard deviation (SD) of the proportion. The t-test was used to compare ADIOL-treated and DMSO-treated animals based on raw data (***$p < 0.001$, ns: non-significant). **(d)** Model indicating that fasting-induced increases in pharyngeal pumping upon re-exposure to food require the steroid hormone ADIOL. Fasting activates NHR-131 in the intestine, which is involved in ADIOL production. In the RIM neuron, ADIOL activates NHR-91 (ERβ), leading to reduced KynA levels and subsequent increases in pharyngeal pumping. **(e and f)**. Learning index of the CR genetic models *mxl-3* **(e)** and *daf-2* **(f)** deficient in NHR-91 or NHR-131 on day 1 of adulthood. Each dot represents animals from a single plate (n = 6 per condition), with 15-332 animals per plate. Error bars indicate the standard deviation (SD) of the learning index. Statistical analysis was performed on the learning index values using one-way ANOVA with Bonferroni's multiple comparisons correction (***$p < 0.001$, **$p < 0.01$, *$p < 0.05$, ns: non-significant). **(g)** Model showing the regulatory connections between CR (caloric restriction) and learning capacity via ADIOL.

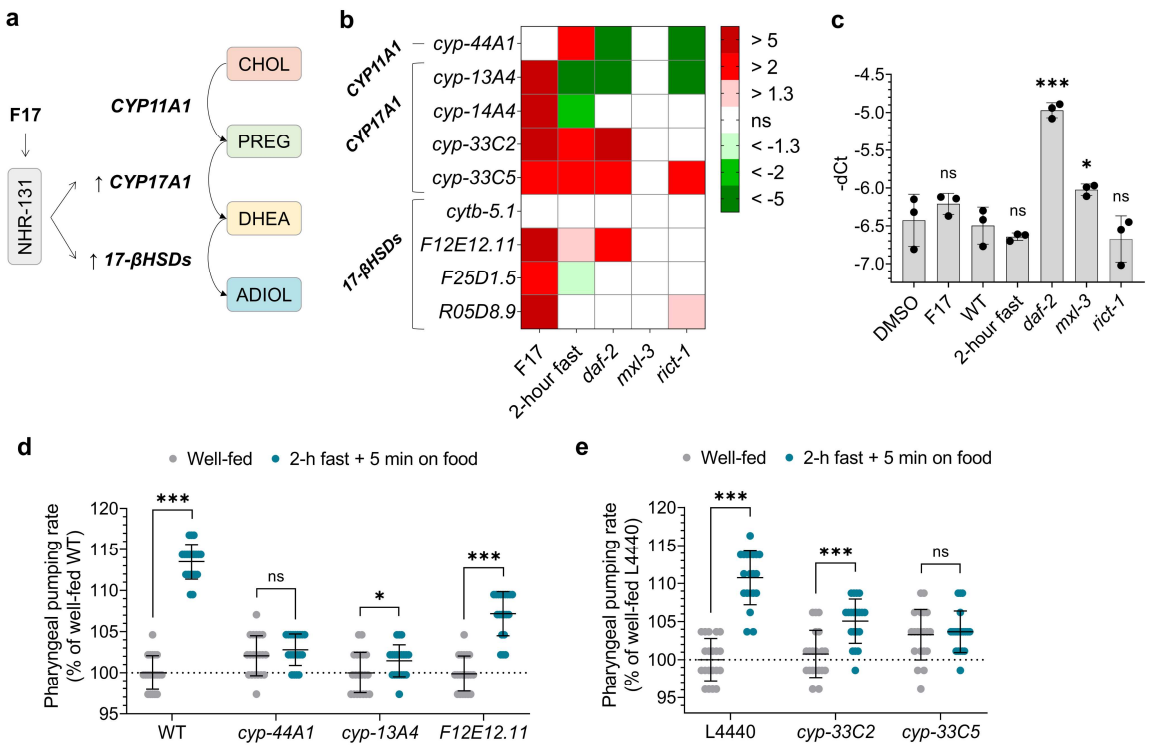

Figure 2. Fasting and genetic models of CR upregulate ADIOL biosynthesis genes. (a) F17-induced activation of NHR-131 promotes ADIOL biosynthesis from cholesterol through upregulation of the *C. elegans* homologs of *CYP17A1* and *17-βHSDs*. The compound F17 activates NHR-131, leading to the upregulation of *CYP17A1* and *17β-HSD* homologs, enzymes that catalyze the conversion of pregnenolone (PREG) to dehydroepiandrosterone (DHEA), and DHEA to ADIOL, respectively. As a result, ADIOL levels increase following F17 treatment (9). **(b)** RT-qPCR analysis of *C. elegans* homologs of the human ADIOL biosynthesis genes *CYP11A1*, *CYP17A1*, and *17β-HSDs* in L4 animals treated with 2.5 μM F17 or under conditions shown. Mean fold change is shown relative to DMSO-treated controls (F17-treated animals) or to well-fed WT animals (2-hour fasting and the mutants shown). The mean was calculated based on results obtained from 2 to 6 biological replicates per condition, with ~300 animals per replicate. Statistical significance was determined using one-way ANOVA with Bonferroni's post hoc test performed on ΔCt values. Non-statistically significant differences (ns) are shown in white. **(c)** RT-qPCR analysis of *nhr-91*, the *C. elegans* ortholog of ERβ, in L4 animals treated with 2.5 μM F17 or under CR. Mean -dCt value is shown. Each dot represents a biological replicate from a single plate (n = 3 per condition; ~300 animals per plate). Error bars represent the standard deviation (SD) of the fold change. Statistical significance was determined using one-way ANOVA with Bonferroni's multiple comparisons correction performed on ΔCt values (**p < 0.001, *p < 0.05, ns: non-significant). **(d and e)** Pharyngeal pumping rate in L4-stage animals under fed and post-fasting conditions. Animals were assessed for the number of pharyngeal pumps over 30 seconds in well-fed conditions

and after a 2-hour fasting period followed by 5 minutes of re-exposure to food. Data are presented as the percentage of the pharyngeal pumping rate normalized to the mean of well-fed WT animals (n = 20 per condition). Error bars indicate the standard deviation (SD) of the proportion. Statistical analysis for the comparison between ADIOL-treated and DMSO-treated animals was performed using the t-test on raw data (***$p < 0.001$, *$p < 0.05$, ns: non-significant). **(d)** WT, *cyp-44A1*, *cyp-13A4*, and *F12E12.11* animals were analyzed. **(e)** WT animals exposed to RNAi clones L4440, *cyp-33C2*, or *cyp-33C5* from the L1 stage.

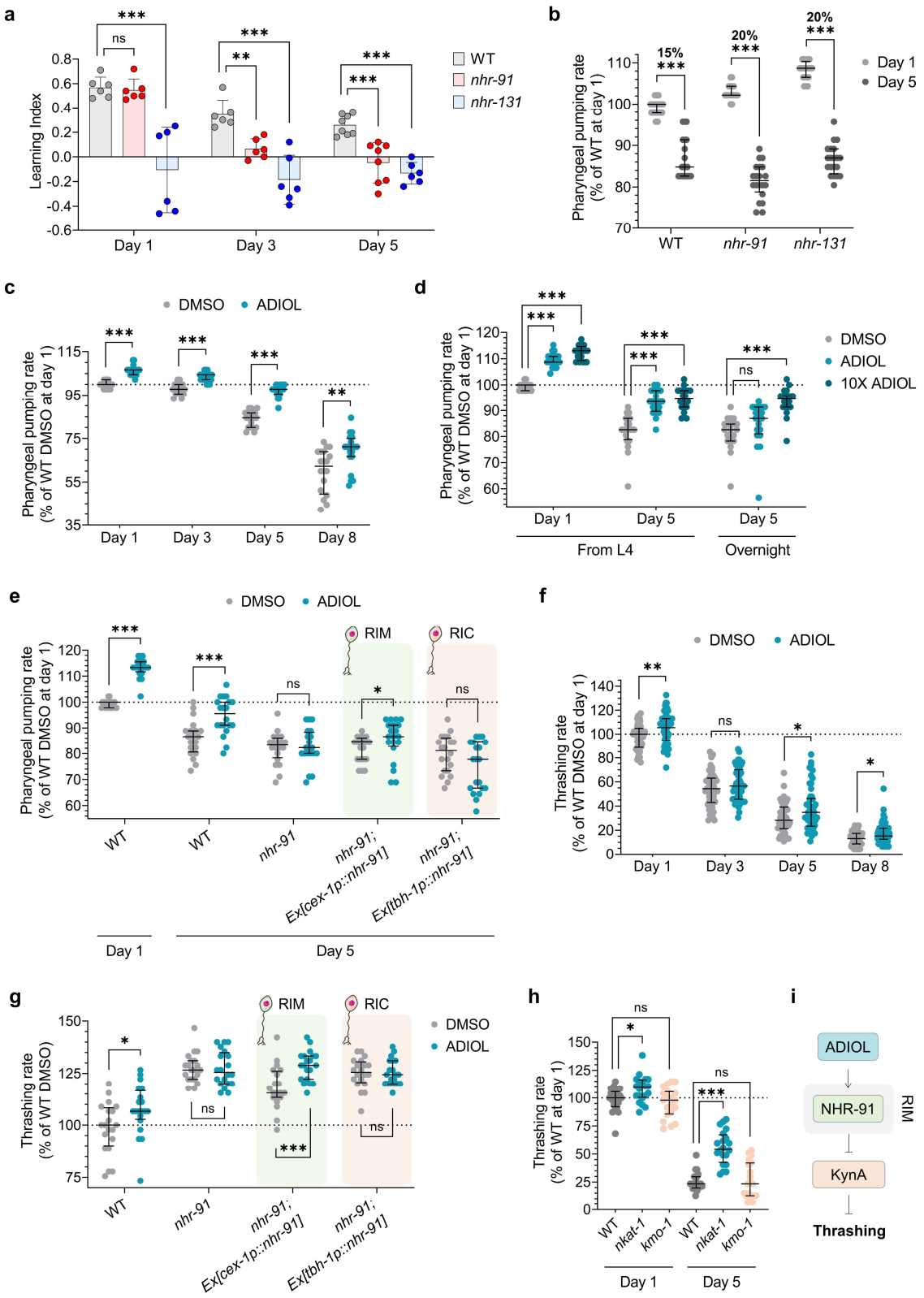

Figure 3. ADIOL promotes neuronal healthspan during aging through KynA reduction. **(a)** Learning index of WT, *nhr-91* and *nhr-131* animals on day 1, 3, and 5 of adulthood. Animals were exposed to 50 μM FUDR starting on day 1 of adulthood. Each dot represents animals from a single plate (n = 6-8 per condition), with 25-232 animals per plate. Error bars indicate

the standard deviation (SD) of the learning index. Statistical analysis was performed on the learning index values using one-way ANOVA with Bonferroni's multiple comparisons correction (***p < 0.001, **p < 0.01, ns: non-significant). **(b-e)** Pharyngeal pumping rate during aging. Pharyngeal pumping was assessed by counting the number of pumps over a 30-second interval. Animals were exposed to 50 μM FUDR starting on day 1 of adulthood. Since pharyngeal pumping data are often non-normally distributed during aging, medians along with interquartile ranges (IQR) are shown in all cases. Although some groups exhibit a normal distribution, medians were used consistently to maintain visual coherence. Statistical analysis was performed based on the normality of the data in each case (see below). **(b)** Pharyngeal pumping rate in WT, *nhr-91* and *nhr-131* animals on day 1 and 5 of adulthood. Data are presented as the percentage of the pharyngeal pumping rate normalized to the median of WT animals on day 1 (n = 20 per condition). The t-test was used to compare day 1 vs day 5 animals based on raw data (***p < 0.001). **(c)** Pharyngeal pumping of WT animals treated with DMSO (vehicle) or 10 nM ADIOL on days 1, 3, 5, and 8 of adulthood. Treatment with DMSO or ADIOL began at the L4 stage. Data are presented as the percentage of the pharyngeal pumping rate normalized to the median of WT DMSO-treated animals on day 1 (n = 20 per condition). Statistical analysis comparing ADIOL-treated and DMSO-treated animals was performed using the t-test (for day 1 and day 3 adults) or the Mann-Whitney U test (for day 5 and day 8 adults), based on raw data (***p < 0.001, **p < 0.01). **(d)** Pharyngeal pumping of WT animals treated with DMSO (vehicle), 10 nM ADIOL or 100 nM ADIOL (10X) on days 1 and 5 of adulthood. For day 5 adults, treatment began either at the L4 stage or on day 4 of adulthood (overnight treatment). Data are presented as the percentage of pharyngeal pumping normalized to the median of WT DMSO-treated day 1 adults (n = 20 per condition). Statistical analysis was performed using one-way ANOVA with Bonferroni's multiple comparisons correction (for day 1 adults) or Mood's median test followed by multiple comparisons (for day 5 adults), based on raw data (***p < 0.001, ns: non-significant). **(e)** Pharyngeal pumping rate in day 5 adults of WT, *nhr-91*, *nhr-91*;Ex[*cex-1p::nhr-91,unc-122::GFP*], and *nhr-91*;Ex[*tbh-1p::nhr-91cDNA::sl2::GFP*] strains treated with DMSO (vehicle) or 10 nM ADIOL from the L4 stage. Data are presented as the percentage of the pharyngeal pumping rate normalized to the median of day 1 DMSO-treated WT animals (n = 20 per condition). Depending on data distribution, either the t-test or the Mann-Whitney U test was used to compare ADIOL-treated and DMSO-treated animals using raw data (***p < 0.001, *p < 0.05, ns: non-significant). **(f-h)** Thrashing rate during aging. Thrashing was assessed by counting the number of thrashes in M9 over a 1-minute interval. Animals were exposed to 50 μM FUDR starting on day 1 of adulthood. Since thrashing data are often non-normally distributed during aging, medians along with interquartile ranges (IQR) are shown in all cases. Although some groups exhibit a normal distribution, medians were used consistently to

maintain visual coherence. Statistical analysis was performed based on the normality of the data in each case (see below). **(f)** Thrashing rate of WT animals treated with DMSO (vehicle) or 10 nM ADIOL on days 1, 3, 5, and 8 of adulthood. Treatment with DMSO or ADIOL began at the L4 stage. Data are presented as the percentage of the thrashing rate normalized to the median of WT DMSO-treated animals on day 1 (n = 50 per condition). Statistical analysis comparing ADIOL-treated and DMSO-treated animals was performed using the t-test (for day 1 and day 3 adults) or the Mann-Whitney U test (for day 5 and day 8 adults), based on raw data (**$p < 0.01$, *$p < 0.05$, ns: non-significant). **(g)** Thrashing rate in day 5 adults of WT, *nhr-91*, *nhr-91*;Ex[*cex-1p::nhr-91,unc-122::GFP*], and *nhr-91*;Ex[*tbh-1p::nhr-91cDNA::sl2::GFP*] strains treated with DMSO (vehicle) or 10 nM ADIOL from the L4 stage. Data are presented as the percentage of the thrashing rate normalized to the median of day 1 DMSO-treated WT animals (n = 20 per condition). The t-test was used to compare ADIOL-treated and DMSO-treated animals based on raw data (***$p < 0.001$, *$p < 0.05$, ns: non-significant). **(h)** Thrashing of WT, *nkat-1* and *kmo-1* animals on day 1 and 5 of adulthood. Data are presented as the percentage of the thrashing rate normalized to the median of day 1 WT animals (n = 20 per condition). Statistical analysis was performed on raw data using one-way ANOVA with Bonferroni's multiple comparisons correction (***$p < 0.001$, *$p < 0.05$, ns: non-significant). **(i)** Model summarizing the effect of ADIOL on thrashing.

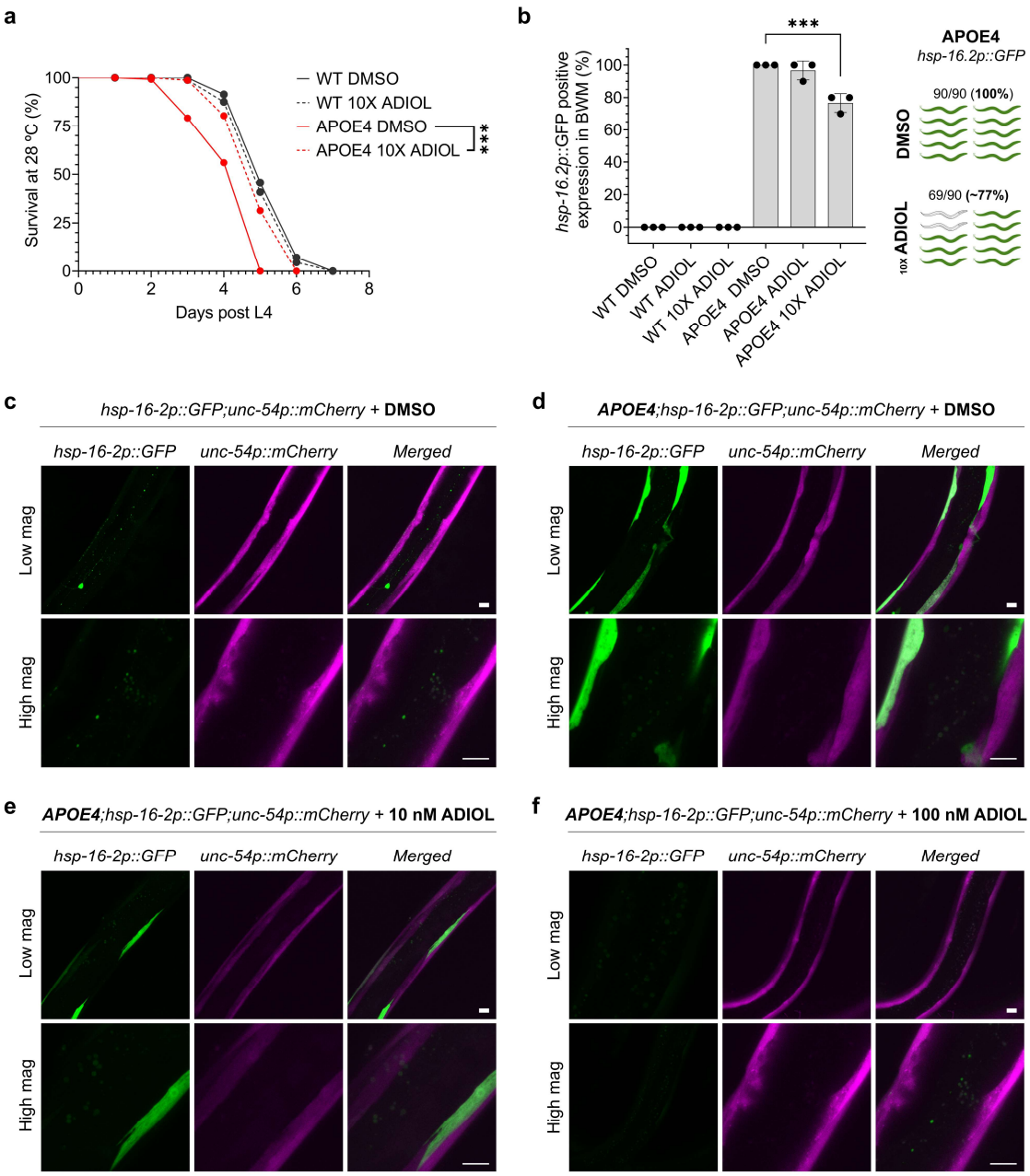

Figure 4. ADIOL suppresses the proteostatic stress induced by the Alzheimer's-associated APOE4 variant. (a) Lifespan curves at 28 °C of WT and APOE4 animals treated with DMSO (vehicle) or 100 nM ADIOL (10X) starting from the embryo stage. Survival was scored daily starting at the L4 stage. Each represents three independent replicates (n = 79-160). Kaplan-Meier survival curves and log-rank test were used for statistical analysis (***p < 0.001). **(b)** Quantification of the percentage of *hsp-16.2p::GFP*-positive expression in the body wall muscle (BWM) of WT and APOE4 animals at day 1 of adulthood. Animals were treated with DMSO (vehicle), 10 nM ADIOL, or 100 nM ADIOL (10X) starting at the embryo stage. Data represent three independent biological replicates (n > 25 animals per replicate). **(c-f)** Representative confocal microscopic images at low and high magnification of *hsp-*

16.2p::GFP;unc-54p::mCherry and APOE4;*hsp-16.2p::GFP;unc-54p::mCherry* animals at day 1 of adulthood. Animals were treated with DMSO (vehicle), 10 nM ADIOL, or 100 nM ADIOL (10X), starting from the embryo stage. Scale bar: 10 μm.

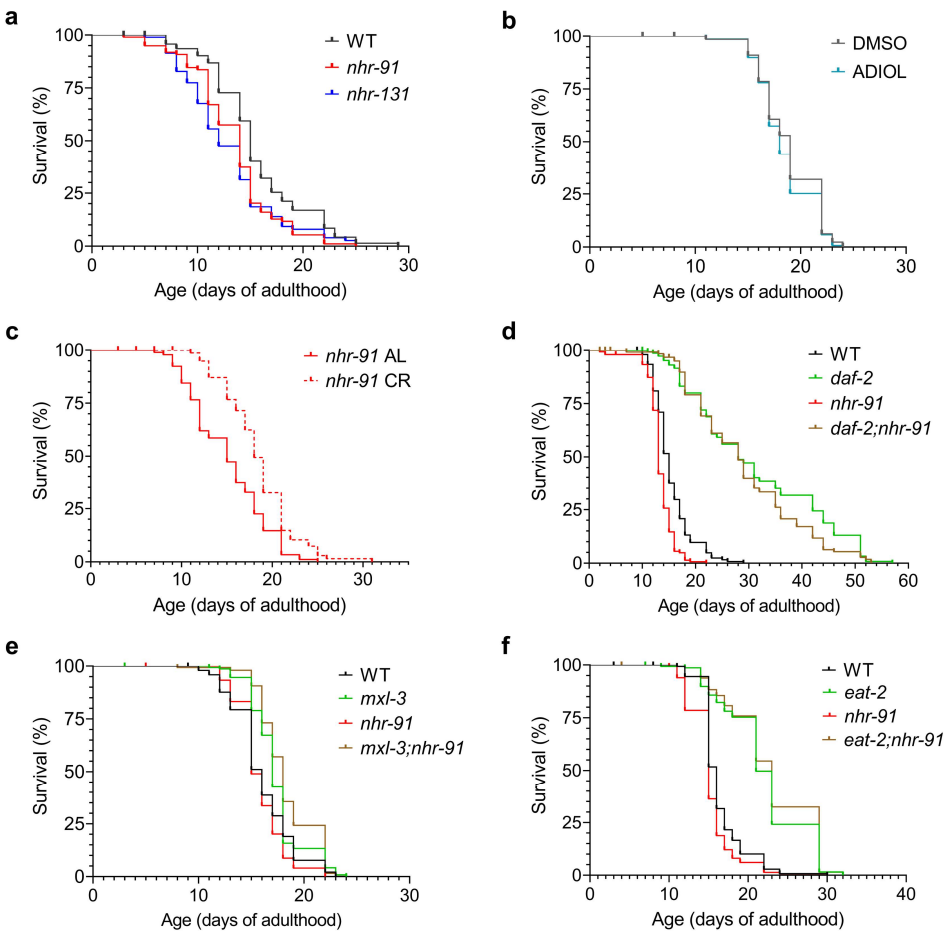

Figure 5. ADIOL has no impact on longevity. (a) Lifespan curves of WT, *nhr-91*, and *nhr-131* animals at 20 ºC. Median survival was 15 days for WT (n = 100), 14 days for *nhr-91* (n = 99), and 12 days for *nhr-131* (n = 96). Kaplan–Meier survival curves were compared using the log-rank test with Bonferroni correction. Statistically significant differences were observed between *nhr-91* and WT (p = 0.002), and between *nhr-131* and WT (p = 0.001). **(b)** Lifespan curves of WT animals treated with DMSO (vehicle) or 10 nM ADIOL from the L4 stage. Median survival was 19 days for DMSO-treated animals (n = 136) and 18 days for ADIOL-treated animals (n = 150). No significant differences between groups were detected according to the log-rank test (p > 0.01). **(c)** Lifespan curves of *nhr-91* animals fed *ad libitum* (AL) or under CR conditions. Median survival was 15 days for animals fed AL (n = 100) and 18 days for animals under CR (n = 100). The log-rank test indicated a statistically significant difference between the two groups (p < 0.001). **(d-f)** Lifespan curves of the CR genetic models *daf-2* **(d)** *mxl-3* **(e)** and *eat-2* **(f)** deficient in NHR-91. Kaplan–Meier survival curves were compared using the log-rank test with Bonferroni correction. **(d)** Median survival was 15 days for WT (n = 154), 28 days for *daf-2* (n = 150), 13 days for *nhr-91* (n = 151), and 28 days for *daf-2;nhr-91* (n = 150). No significant differences between *daf-2* and *daf-2;nhr-91* mutants were detected according to the log-rank test (p > 0.01). **(e)** Median survival was 16 days for WT (n = 150), 17 days for

mxl-3 (n = 150), 15 days for *nhr-91* (n = 150), and 18 days for *mxl-3;nhr-91* (n = 150). No significant differences between *mxl-3* and *mxl-3;nhr-91* mutants were detected according to the log-rank test ($p > 0.01$). **(f)** Median survival was 16 days for WT (n = 150), 21 days for *eat-2* (n = 150), 15 days for *nhr-91* (n = 150), and 23 days for *eat-2;nhr-91* (n = 150). No significant differences between *eat-2* and *eat-2;nhr-91* mutants were detected according to the log-rank test ($p > 0.01$).